RSC Advances

ROYAL SOCIETY OF CHEMISTRY

www.rsc.org/advances

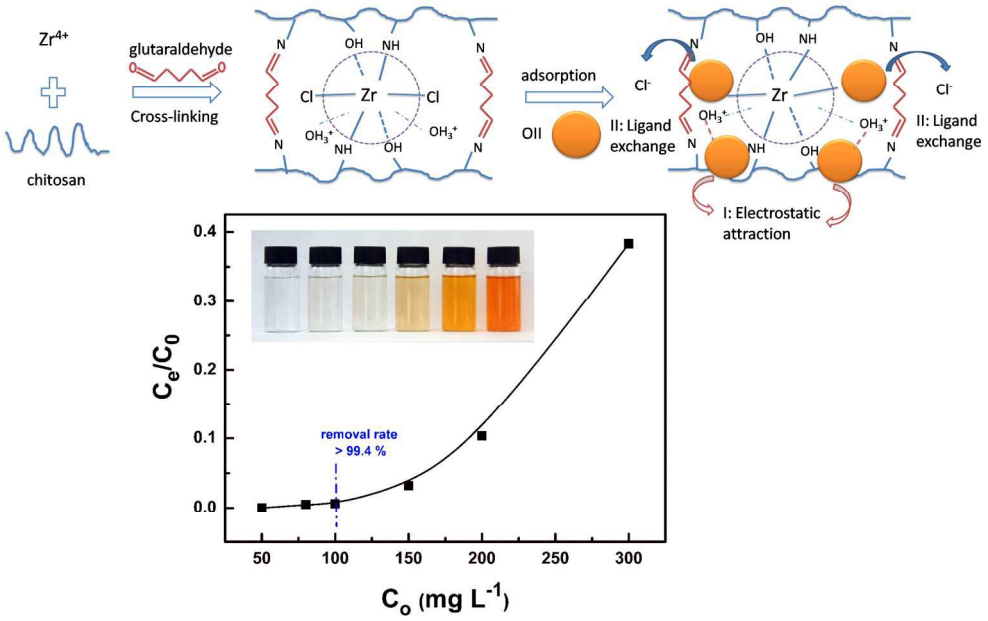

635x405mm (96 x 96 DPI)

Effective removal of azo-dye orange II from aqueous solution by zirconium-based chitosan microcomposite adsorbent

Lingfan Zhang [a,b], Linxiao Chen [a], Xin Liu [a*] and Wenqing Zhang [a**]

[a] School of Chemistry and Molecular Engineering, East China University of Science and Technology, Shanghai 200237, PR China

[b] Research Center of Analysis and Test, East China University of Science and Technology, Shanghai 200237, PR China

[*] Corresponding author:

Xin Liu, E-mail address: liuxin@ecust.edu.cn

[**] Corresponding author:

Wenqing Zhang, E-mail address: zhwqing@ecust.edu.cn

Tel.: +86-21-64253225

Fax: +86-21-64252947

Abstract:

In this study, zirconium-based chitosan (CTS@Zr) microcomposite was prepared and employed as an efficient adsorbent for the removal of Orange II dye from aqueous solution. The microcomposite was characterized by BET, FT-IR, XRD, SEM and EDS. Various parameters including solution pH, contact time, temperature and initial dye concentration were systematically investigated. The results showed that the adsorption process was pH dependent and the optimum condition was at pH 2.0. Adsorption kinetics followed the pseudo-second order model and thermodynamic constant values demonstrated that the adsorption process of Orange II dye onto CTS@Zr microcomposite was feasible, spontaneous ($\Delta G^o < 0$) and endothermic ($\Delta H^o > 0$) under the examined conditions. Equilibrium isotherms showed a good fit with Langmuir isotherm equation for the monolayer adsorption process and the maximum adsorption capacity was calculated for 926 mg g^{-1}. More importantly, the removal rate was higher than 99.4% when initial dye concentration was less 100 mg L^{-1} (0.20 g L^{-1} dosage), indicating that the CTS@Zr microcomposite exhibited excellent efficiency for the removal of Orange II dye. Moreover, the Orange II loaded CTS@Zr microcomposite adsorbent was easily regenerated by using 0.05 M NaOH within 10 min and the adsorption capacity still remained 98% after six regeneration cycles. The mechanisms of adsorption were attributed to electrostatic attraction and ligand exchange reaction between CTS@Zr and Dye-SO_3^- anions. Therefore, the CTS@Zr microcomposite adsorbent possesses a great potential for the removal of Orange II dyes from aqueous solution.

Keywords: Chitosan, Microcomposite, Adsorption, Orange II dye

1. Introduction

Azo dyes, a class of synthetic organic dyes, are widely used as colorants in textile, leather, cosmetics, paper and electroplating industries.[1] Along with the increase in dyes used, it will inevitably produce a considerable amount of dye effluents into the environment. These dyes generally have complex aromatic structures which are stable to oxidizing agents, resistant to aerobic digestion and even non-degradable under light or heat.[2] Additionally, most of these dyes are known to be toxic, carcinogenic, mutagenic and teratogenic, which can cause serious hazard to aquatic living organisms and even to human.[3] Hence, removal of dyes from wastewaters before discharging emerges a major challenge from environmental point of view.

Various physical, chemical and biological methods including adsorption, coagulation, membrane filtration, chemical oxidation, photo-degradation, aerobic or anaerobic treatment have been employed to treat dyes from colored wastewater. Among these methods, adsorption has been found to be one of the best available techniques for dye removal because of its easy operation, low cost and high effectiveness.[4-6] As a result, numerous adsorbents including activated carbons[7], graphene oxide[8], zeolites[9,10], clays materials[11,12], macroalga[3] and polymeric materials[13] have been used for the purpose of dye removal from wastewater.

Recently, many researchers have studied the feasibility of using low-cost biomass for treatment of dye containing wastewater, such as chitosan[14-16]. Chitosan possesses a large of functional groups, i.e. amine (-NH_2) and hydroxyl (-OH) groups, which show

high adsorption potential for dyes molecules. However, pure chitosan has some obvious disadvantages, such as low adsorption capacity, difficult recovery and pH sensitively, which limit its application on the industrial scale. To overcome these limitations, modification of chitosan by physical and chemical methods such as mixing[1,17], cross-linking[18,19] and grafting[20,21] with activated compounds are always been employed to improve its stability and adsorption capacities. However, these adsorbents inevitably occupied many activated sites such $–NH_2$ groups and produced certain limitations like the lack of electrostatic interactions with ionic dyes. Therefore, further development of new adsorbents, which carry permanent charges, are a worthwhile target to improve the adsorption efficiency.

More recently, Zr(IV) ions were introduced into advanced adsorbents and applied for pollutants removal by many researches[4,22,23], which can not only make the prepared materials more stable but also improve the adsorption performances. This is because tetravalent zirconium ions are easily hydrolyzed to form tetranuclear ions or octanuclear species, resulting in a large number of hydroxyl ions and water molecules, which can take part in the ligand exchange reaction with the target pollutant.[24] Incorporation the biopolymer chitosan to inorganic Zr(IV) ions to obtain the inorganic-biopolymer complex materials of Zr-based/chitosan may preserve or even improve the major features of each phase in the composite materials, and furthermore, new properties may come from the synergy of both components. Thus, utilizing a strategy to prepare inorganic-biopolymer composite material of Zr-based/chitosan for water treatment would be of significance.

In this study, we reported on the development, characterization and application of inorganic-biopolymer materials of Zr-based/chitosan microcomposite through a co-precipitation method and spray technique as an adsorbent to removal of organic dyes pollutants. The obtained microcomposite can afford electrostatic charges and enhance electrostatic attraction with anionic dyes, resulting in significantly higher adsorption efficiency. Orange II azo-dye serves as a model compound of the harmful and water soluble organic dyes pollutants, which are inexpensive and widely used in textile, pulp and paper industries and harmful to the environment. The effects of various parameters on the adsorption capacity of Orange II with CTS@Zr microcomposite were studied by batch experiment. The kinetics and isotherm models were applied to study the adsorption mechanism. The CTS@Zr microcomposite can be suggested as a suitable material for the efficient removal of organic dyes pollutants from aqueous solution.

2. Experimental Section

2.1. Chemicals.

Chitosan (CTS), which had a 91% degree of deacetylation, was supplied by Shanghai Weikang Biological (China). Glutaraldehyde was purchased from Merck (China). The structures of chitosan and glutaraldehyde were shown in scheme 1. Zirconium oxychloride octahydrate ($ZrOCl_2 \cdot 8H_2O$, analytical grade) was purchased from Sinopharm Chemical Reagent, Ltd (China). Stock solution (1000 mg L^{-1}) was prepared by dissolving 0.10 g Orange II (analytical grade, Sigma-Aldrich) in 100 mL de-ionized water. All work solutions were derived through appropriate dilution of the

stock solution with distilled water. Acetic acid, hydrochloric acid (HCl), sodium hydrate (NaOH) and other chemicals used in this work were all A.R.- grade reagents and also supplied by Sinopharm Chemical Reagent, Ltd (China). Distilled water was used in all experiments.

Please insert Scheme 1 here

2.2. Synthesis of Zr-based chitosan microcomposite adsorbent

Zr-based chitosan (CTS@Zr) microcomposite adsorbent was synthesized by using co-precipitation method and spray technique. In detail, 3.22 g CTS powder was dissolved into 100 mL 2% (v/v) acetic acid aqueous solution. Then, 0.10 M $ZrOCl_2 \cdot 8H_2O$ (3.22 g) was slowly added with stirring for 2 h at room temperature to obtain a homogeneous solution. Subsequently, sodium hydroxide (2.0 M, 30 mL) solution as pH adjusted reagent was sprayed into the mixture using a nebulizer (an accessory of ICP-OES) under a continuous stirring (200 rpm) and the CTS@Zr microcomposite was precipitated. After that, in order to improve microcomposite stability, 5 mL 5% of glutaraldehyde aqueous solution as cross-linking agent was added and stirred vigorously for another 2 h. At last, the microcomposite was washed with distilled water to neutral pH and dried at 50 ^{o}C for 2 days. Amount of Zr and Cl in final microcomposite were 27.5% and 2.61% (wt%), respectively. The obtained CTS@Zr microcomposite was used for Orange II adsorption studies. For comparison, different amount of $ZrOCl_2 \cdot 8H_2O$ (0.0, 0.05 and 0.15 M) were added to prepare the composites at the same condition.

2.3.Characterization

The functional groups of CTS, CTS@Zr before and after Orange II adsorption were analyzed by Fourier transform infrared spectroscopy (FT-IR, Nicolet 6700, Thermo Electron, USA). Wide-angle X-ray diffraction (XRD) measurements were carried out using an XRD diffractometer (D/MAX 2550 VB/PC, Rigaku corporation). The patterns with the Cu Kα radiation (λ = 0.154 nm) at 40 kV and 30 mA were recorded in the region of 2θ from 3 ^{o}C to 80 ^{o}C. The morphological structure and surface elements of CTS@Zr microcomposite were examined by using a scanning electronic microscopy (SEM, JSM-6360LV, Japan) with an energy dispersive X-ray spectroscopy (EDS, Falcon energy dispersive X-ray analyzer). The Brunauer-Emmett-Teller (BET) surface area was measured on a Micromeritics ASAP 2010 analyzer. The inductively coupled plasma optical emission spectroscopy (ICP-OES, 725ES, Aglient, USA) was used to determine the leaching concentration of Zr^{4+} in solutions. The zeta potential was determined (Electrophoretic spectroscopy, JS84H, Shanghai Zhongchen Digital Instrument Co., Ltd., China) by mixing 50 mg samples with 100 mL 0.01 mol L^{-1} KNO_3 solution with pH values adjusted between 1 and 11 by adding 0.5 mol L^{-1} HNO_3 or 0.5 mol L^{-1} NaOH.

2.4. Adsorption studies

The adsorption of Orange II on CTS@Zr microcomposite was studied in the batch mode and effect of different parameters, including solution pH (1 ~ 11), contact time (0 ~ 36 h), temperature (4 ^{o}C ~ 40 ^{o}C, carried out in fridge and incubator) and initial Orange II concentration (50 ~ 300 mg L^{-1}) were assessed. In a typical experiment, 20 mg adsorbent was added to a conical flask containing 100 mL solution of Orange II

(100 mg L^{-1}). The pH value of solution was adjusted with 0.5 M HCl or 0.5 M NaOH to obtain the desired values. Then the conical flask was placed to the shaker at 150 rpm for 12 h, followed by filtration to remove the adsorbent. The experiments were carried out by varying the solution temperature and initial Orange II concentration for investigation of the isotherm at the identical pH value. For kinetics studies, samples were taken to determine the concentration of Orange II at different time intervals. The concentration of Orange II in the filtrate was determined by using JASCO V-570 UV/VIS spectrophotometer at the maximum absorption (λ = 483 nm). The amount of adsorbed dye on CTS@Zr microcomposite was calculated according to the following equation:

$$q_e = \frac{C_o - C_e}{m} V \qquad q_t = \frac{C_o - C_t}{m} V \qquad (1)$$

Where q_e and q_t(mg g^{-1}) are the adsorption capacity values in solid phase at equilibrium and t time. C_o, C_t and C_e (mg L^{-1}) are the initial concentration, t time and equilibrium concentration of Orange II in the liquid phase, respectively. V (L) is the volume of the solution and m (g) is the weight of CTS@Zr microcomposite. The Orange II dye concentrations were obtained through Beer-Lambert Law in which the absorbance value (λ = 483 nm) for Orange II versus concentration obeys a linear relationship.

2.5. Desorption and regeneration studies

After adsorption, the saturated Orange II loaded CTS@Zr microcomposite was removed from the solution and rinsed with water. For regeneration, the adsorbent was immersed in the 0.05 M of NaOH and sharked for 30 min. Then, the CTS@Zr

microcomposite was removed from the solution and wash with water. The composite was dried at 30℃ before being reused in the next cycle. The adsorption-regeneration cycles were repeated for six times with the Orange II adsorption capacity analysis.

3. Results and discussion

3.1. Characterization

Please insert Fig. 1 here

FT-IR spectra of CTS, CTS@Zr and Orange II loaded CTS@Zr (CTS@Zr-OII) are shown in Fig.1A. Compared to CTS (1657 cm^{-1}), the FT-IR spectrum of CTS@Zr showed the $–NH_2$ bending at 1623 cm^{-1} with a shift of 34 cm^{-1}. The two bands at 1154 and 1080 cm^{-1} corresponding to secondary and primary –OH stretching were merged into one band with 6 cm^{-1} shifted in CTS@Zr FT-IR spectrum.[25] These shifts were due to the interaction of –OH and $–NH_2$ groups with tetravalent Zr^{4+} ions. Besides, two new peaks were found at 644 and 463 cm^{-1}, which may be attributed to Zr-N vibration and Zr-hydroxy-bridged complex stretch.[26] Furthermore, the peak at 1378 cm^{-1} corresponded to the stretching vibration of C-N (amide III in CTS) was almost disappeared in CTS@Zr. And the other peak at 1256 cm^{-1}, which corresponds to C-N functionality, weakened after cross-linking procedure probably as a result of the bonding interaction of the glutaradehyde and C-N groups. [27] These changes indicated that Zr^{4+} ions successfully bended onto amino and hydroxyl groups of CTS and the cross-linking reaction was also occurred between C-N and glutaradehyde. After Orange II adsorption onto CTS@Zr microcomposite, the several bands were observed at 1506, 1210 and 1027 cm^{-1}, which were corresponded to C=C stretching vibration,

N-N stretching vibration and -O-S(O2)- symmetric vibration in Orange II, respectively[9], indicating that Orange II was successfully adsorbed on the surface of CTS@Zr microcomposite. The XRD patterns of CTS, CTS@Zr and CTS@Zr-OII were recorded in the range of $2\theta = 3 \sim 80^{o}$ and shown in Fig. 1B. From the figure of CTS, the characteristic peaks at 10.3^{o}, 19.8^{o}, 22.0^{o}, 35.6^{o} were separately attributed to (001), (100), (101), (002) planes, respectively.[28] However, the XRD spectrum of CTS@Zr microcomposite showed only one extraordinary broad peak at 28.0^{o}, which might be due to the conjugation of Zr^{4+} and chitosan resulted in decreasing the crystalline nature to some extent. After Orange II adsorption, only one broad peak was also found at 27.5^{o}. The results demonstrated that CTS@Zr microcomposite belonged to amorphous materials. Besides, the SEM images and EDS analysis for CTS@Zr microcomposite before and after Orange II adsorption were conducted and shown in Fig. 1C ~ F. Fig. 1C showed that the surface of CTS@Zr microcomposite was non-porous and random, which consisted with the data of BET surface area (6.24 m^2/g, listed in Table 1). After adsorption, the rough structure in Fig. 1D was formed due to the accumulation of the Orange II by adsorption mechanism. The EDS spectrum of CTS@Zr microcomposite showed the presence of C, N, O, Cl and Zr and the quantitative elemental composition was listed in Table 1, which confirmed the incorporation of Zr^{4+} ions into chitosan matrix. More importantly, the presence of element S peak demonstrated that Orange II dyes were absorbed onto the surface of CTS@Zr microcomposite. The content of S reached as high as 5.53 % (see Table 1), indicating that CTS@Zr microcomposite had high adsorption capacity for removal

Orange II dyes. Interestingly, the peak of element Cl was disappeared after adsorption, suggesting that there was a ligand exchange reaction between the coordinated Cl and dye-SO_3^-.

Please insert Table 1 here

3.2. Effects of pH

Please insert Fig. 2 here

The pH significantly influences the overall adsorption process, since it affects not only the surface charges of adsorbent but species of dyes ions in solution. The effects of pH on the adsorption of Orange II dyes onto CTS@Zr microcomposite were studied by varying the pH from 1 to 11, while the initial dye concentration, temperature, adsorbent dosage and contact time were kept constant at 50 and 100 mg L^{-1}, 30 ^oC, 20 mg and 10 h, respectively. The plot of dye adsorption capacity versus pH was shown in Fig. 2A. It was noted that maximum adsorption capacities for Orange II on CTS@Zr microcomposite were obtained at pH 2 for initial concentrations of 50 and 100 mg L^{-1}, then decreased with increasing the initial solution of pH from 3 ~ 11. In aqueous solution, Orange II can be ionized and converted to anionic dyes ions with sulfate groups.

$$\mathrm{Dye-SO_3Na \rightarrow Dye-SO_3^- + Na^+} \qquad (2)$$

In acidic solution, the element of Zr on CTS@Zr microcomposite can be protonated to Zr-OH_3^+ by hydrogen ions (H^+). Higher adsorption capacity obtained at lower pH might be due to the electrostatic interaction between negatively charged Dye-SO_3^- ions and positively charged Zr^{4+} and Zr-OH_3^+ on adsorbent surface. To further

understand the influence of pH on the Orange II removal process, we measured the values of zeta potential of CTS@Zr microcomposite at different pH and shown them in Fig. 2A. From this figure, the point zero charge of CTS@Zr microcomposite was found to be 3.5, indication that at pH below 3.5 the microcomposite was carrying positive charges due to the protonation of Zr-OH_3^+ groups. Orange II molecules have the negative charges because of the anionic sulfonate groups. Hence, the strong electrostatic forces between the protonated adsorbent and negatively charge Orange II anions occurred at low pH value, leading to the improved Orange II adsorption. However, at pH above 3.5, a lower adsorption capacity was expected because of the repulsive forces between negatively charged of adsorbent and anions adsorbate. Additionally, at solution pH = 1, the decrease of adsorption capacity was due to small amount of Zr^{4+} (0.023 mg L^{-1}, determined by ICP-OES) leached into solution, demonstrating that the CTS@Zr microcomposite would be dissolved to some extent in such condition. To further justify this phenomenon, the different amount of Zr^{4+} (0.05, 0.10 and 0.15 mg L^{-1}) were employed to prepare the composites to remove Orange II, the data was shown in Fig. 2B. From this figure, the maximum adsorption capacity was obtained at 0.1 mg L^{-1} Zr^{4+}. When Zr^{4+} was less than 0.1 mg L^{-1}, the adsorption sites were not enough to absorb the Orange II molecules. On the other hand, however, the more Zr^{4+} ions were leached into solution due to more zirconium hydroxide formed during the preparation, which leading to decrease the adsorption capacity. Under alkaline conditions, the increased OH^- ions presented in the solution implied competition of the OH^- ions with anions dye molecules, which reduced the

adsorption of Orange II.

3.3. Adsorption Kinetics and thermodynamics

Please insert Fig. 3 here

The kinetic parameters are helpful in the prediction of adsorption rate, which gives important information for the application of adsorbents. For this study, the effect of contact time on Orange II adsorption was investigated in the initial concentration of 200 mg L^{-1} (100 mL) containing fixed adsorbent amounts (20 mg) at different temperature (277, 293, 303 and 313 K). As it can be seen in Fig. 3A, all the adsorption kinetic curves appeared rapid rising at the beginning stage then approached equilibrium within approximately12 h. To analyze the adsorption rate of Orange II on CTS@Zr microcomposite, pseudo-first-order (PF) and pseudo-second-order (PS) kinetic modes were applied to study the experimental data. The PF and PS models were given as equations (3) and (4), respectively:

PF model: $\log(q_e - q_t) = \log q_e - \frac{k_1}{2.303} t$ (3)

PS model: $\frac{t}{q_t} = \frac{1}{k_2 q_e^2} + \frac{t}{q_e}$ (4)

Where q_e and q_t (mg g^{-1}) are the amounts Orange II adsorbed onto the CTS@Zr microcomposite at equilibrium and at time t, respectively. k_1 (min^{-1}) and k_2 (g (mg min)$^{-1}$) are the PF and PS rate constant of adsorption. The value of parameters on both models was calculated from the intercept and slop of the curves.

After curve-fitting, it was noted that the PF models was not well fitted the experimental data (the figure was not given), however, the PS models did well. The linearized forms of PS models for the sorption of Orange II onto CTS@Zr

309 microcomposite at different temperature were presented in Fig.3B and their
310 parameters were listed in Table 2. The values of the correlation coefficient (R^2) for the
311 PS models were higher than 0.99 for all the conditions, and the adsorption capacities
312 calculated by the model (q_{m2}) were also closer to those determined by experiments
313 (q_{exp}). These results indicated that it was feasible for the applicability of PS kinetic
314 model to describe the adsorption process of Orange II on CTS@Zr microcomposite.
315 The PS model is based on the assumption that the rate-controlling step may be a
316 chemical sorption involving valence forces through exchange of electrons between
317 adsorbent and adsorbate.[29] In fact, CTS@Zr microcomposite possessed many Cl
318 ligand groups, which would give more reaction sites to exchange anions dyes from
319 solution in order to enhance the adsorption capacity of Orange II onto the adsorbents.

320 **Please insert Table 2 here**

321 The thermodynamic parameters such as Gibbs free energy change (ΔG^0),
322 standard enthalpy change (ΔH^0) and standard entropy change (ΔS^0) were also studied
323 to further understand the effect of temperature on the adsorption. The experiments
324 were conducted at 277, 293, 303 and 313 K to investigate the effect of temperature
325 with 200 mg L^{-1} of initial Orange II concentration and 20 mg of adsorbent dosage.
326 The values of thermodynamic parameters associated with adsorption were calculated
327 by means of Van't Hoff's equations, were given as follows:

328 $$\Delta G^0 = -RT \ln K_L \qquad (5)$$

329 $$\ln K_L = -\frac{\Delta H^0}{RT} + \frac{\Delta S^0}{R} \qquad (6)$$

330 Where K_L is the adsorption distribution coefficient and the value was calculated by

the ratio of q_e to C_e at different temperatures. R is the universal gas constant (8.314 J mol^{-1} K^{-1}) and T is the absolute temperature in Kelvin.

The plot of ln K_L as a function of 1/T (Fig. 3C) yielded a straight line from which ΔH^0 and ΔS^0 were calculated from the slope and intercept, respectively. The values of ΔG^0, ΔH^0 and ΔS^0 were presented in Table 2. The overall ΔG^0 during the adsorption process at 277, 293, 303, 313 K were negative, corresponding to a spontaneous and thermodynamically favorable process of adsorption of Orange II onto CTS@Zr microcomposite. As the temperature increased from 277 to 313 K, the ΔG^0 values also increased, indicating that more driving force occurred at higher temperatures and hence resulted in more adsorption capacity for Orange II. The positive value of ΔH^0 (57.3 kJ mol^{-1}) suggested that the adsorption process was endothermic in nature, and the positive value of ΔS^0 (0.223 kJ $(mol \cdot K)^{-1}$) showed the increased randomness state at the solid-solution interface during dye adsorption process.

3.4. Adsorption Isotherms for Orange II removal

Please insert Fig. 4 here

Isotherms are the equilibrium relations between the concentration of adsorbate on the solid phase and its concentration in the liquid phase. The equilibrium studies were conducted for 20 mg of CTS@Zr microcomposite in 100 mL solutions at 303 K, where the concentration of Orange II was varied from 50 to 300 mg L^{-1}. The adsorption capacity of Orange II as a function of equilibrium Orange II concentrations were plotted in Fig.4A. It was observed that the adsorption capacity of Orange II increased from 250 to 926 mg g^{-1} when the initial Orange II concentration increased

from 50 to 300 mg L^{-1}. Beside, the curve of C_e/C_o vs. C_o was also depicted in Fig. 4B. It was found that the removal rate of Orange II decreased from 100% to 63% (The images of Fig. 4C demonstrated the removal effect with different initial dyes concentrations). The decrease of removal percentage might be due to the saturation of binding sites at higher dyes concentration. However, when the initial Orange II concentration was lower than 100 mg L^{-1}, 99.4% of Orange II was removed from the solution, indicating that CTS@Zr microcomposite can be used as an effective adsorbent to treat polluted water with low concentration of Orange II (< 100 mg L^{-1}).

For further interpretation of the adsorption data, three common adsorption isotherm models were employed, such as the Langmuir, Freundlich and Temkin models, which can be represented in a linear way as equation (7) ~ (9):

Langmuir model: $$\frac{C_e}{q_e} = \frac{1}{k_L q_{max}} + \frac{C_e}{q_{max}} \quad (7)$$

Freundlich model: $$\ln q_e = \ln k_F + \frac{1}{n} \ln C_e \quad (8)$$

Temkin model: $$q_e = B \ln A + B \ln C_e \quad (9)$$

Where k_L is the Langmuir adsorption constant (L mg^{-1}), related to the adsorption free energy. k_F (L mg^{-1}) and n are Freundlich constants corresponding with adsorption capacity and adsorption intensity, respectively. B = RT/b, where b is a constant, is related to the heat of adsorption and A is the equilibrium binding constant (L mg^{-1}).

The isotherm constants and correlation coefficients for Langmuir, Freundlich and Temkin models are listed in Table 3. The regression coefficient (R^2 = 0.999) values showed better fitting of experimental data towards Langmuir isotherm. This suggested that the adsorption process as a monolayer adsorption on a homogeneous surface.

Besides, the degree of suitability of adsorbent towards Orange II was estimated from the values of separation factor constant (R_L), which can be calculated from the following equation:

$$R_L = \frac{1}{1+k_L C_0} \qquad (10)$$

Where k_L is the Langmuir isotherm constant and C_o is the initial dye concentration. The value of R_L shows that adsorption Orange II on CTS@Zr microcomposite is unfavorable ($R_L > 1$), linear ($R_L = 1$), favorable ($0 < R_L < 1$) or irreversible ($R_L = 0$). In this study, the R_L values were between 0.02 and 0.11 (see Table 3), implying favorable adsorption of the Orange II on CTS@Zr microcomposite. Moreover, from Langmuir adsorption isotherm, the maximum adsorption capacity (q_{max}) of the CTS@Zr microcomposite for Orange II was estimated to be 926 mg g^{-1}. To evaluate the Orange II adsorption performance of CTS@Zr microcomposite, the adsorption capacity was compared to other reported materials and summarized in Table 4. Obviously, CTS@Zr microcomposite had a high adsorption capacity towards Orange II, which suggested that CTS@Zr microcomposite can be potentially used as an adsorbent for decontamination of dyes-polluted water.

Please insert Table 3 and Table 4 here

3.5. Merits of CTS@Zr microcomposite

Please insert Fig. 5 here and Table 5 here

In order to exhibit the merits of CTS@Zr microcomposite, the adsorption performance for Orange II dyes were further studied on CTS, chitosan cross-linked by glutaraldehyde (CTS-GL) and CTS@Zr. As shown in this Fig. 5, it was obvious that

CTS@Zr exhibited higher adsorption capacity compared to CTS and CTS-GL. The original CTS had a certain adsorption capacity for Orange II dyes removal, but CTS itself can be dissolved in acid medium (pH < 5), which limited its application in dyes removal. After cross-linking reaction by glutaraldehyde, CTS-GL owned well stability in acidic medium, however, the adsorption capacity was less than CTS. This was attributed to occupy the amine groups on CTS through cross-linking reaction and leaded to a decrease the adsorption capacities for Orange II. Besides, the equilibrium time, adsorption capacity and remove rate were also carried out in the initial concentration of 100 mg L^{-1} Orange II (100 mL) and dosage of 20 mg at 303 K. The results were list in Table 5. It was also found that the adsorption of CTS@Zr for Orange II dyes exhibited better performances than CTS and CTS-GL.

3.6. Regeneration study

Please insert Fig. 6 here

For practical applications, recovery and regeneration of adsorbent is very important feature. In this study, the adsorption and desorption process were repeated to examine the potential application of the CTS@Zr microcomposite for recycling. Importantly, based on the pH dependence of the adsorption capacity of Orange II loaded on CTS@Zr microcomposite as shown in Fig. 2A, Orange II was released almost fully at a pH higher than 11.0. Therefore, the Orange II desorption process was carried out in a 0.05 mol L^{-1} NaOH aqueous solution as shown in Fig. 6. From this figure, the desorption rate (DR) was rapid at first stage and the fully desorption was obtained within only 10 min. Furthermore, to investigate the reusability of CTS@Zr

microcompoiste, adsorption-desorption cycle was repeated six times and the results were shown in Fig. 6 (insert figure), which demonstrated the adsorption capacities of CTS@Zr microcomposite still maintained above 98% after the 6^{th} adsorption-desorption cycle. Therefore, it was concluded that CTS@Zr microcomposite can be renewed easily with NaOH solution and used repeatedly as an efficient adsorbent for practical dyeing wastewater treatment.

3.7. Adsorption Mechanism

Please insert Scheme 2 here

Based on the above analysis, the functional groups on the surface of CTS@Zr microcomposite played more important role for Orange II dyes adsorption under the experimental conditions. The Zr element on the CTS@Zr could be protonated and positively charged to form Zr^{4+} in an acidic medium. The adsorption of Orange II on CTS@Zr microcomposite was based on electrostatic interaction between the Zr^{4+} cations and the negatively charged sulfonic groups of the Orange II molecules. (Dye-SO_3^-). On the other hand, the ligand of Cl on the surface of CTS@Zr microcomposite was also exchanged with Dye-SO_3^- and formed CTS@Zr-SO_3-Dye complex, which was confirmed by the disappearance of Cl in EDS analyses. Therefore, the proposed possible adsorption for Orange II removal by the CTS@Zr microcomposite was presented in Scheme 2. The anionic Dye-SO_3^- dyes were adsorbed onto the CTS@Zr microcomposite by ligand exchange of Cl and the electrostatic attraction of protonated sites of Zr^{4+} center.

4. Conclusions

In this work, the Zr-based chitosan microcomposite adsorbent was prepared and characterized using several methods. A comprehensive study was conducted on its adsorption capacity for the removal of dye pollutant (Orange II) from aqueous solution. The proposed microcomposite had a high efficient removal capacity for Orange II at the condition of pH 2.0. The experimental data of Orange II on the CTS@Zr microcomposite can be described by the pseudo-second-order kinetics and the Langmuir isotherm model, with remarkable maximum adsorption capacity of 962 mg g^{-1}, which was higher than other reported literatures. The nature of adsorption was feasible, spontaneous and endothermic. EDS and pH studies showed that the adsorption mechanism were electrostatic attraction and ligand exchange reaction between CTS@Zr and Dye-SO_3^- ions. It is believed that CTS@Zr microcomposite can be used as a good promising adsorbent for removal of Orange II dyes from wastewater.

Acknowledgement

We are grateful for the financial support by National Natural Science Foundation of China (Grant No. 21407050) and the Fundamental Research Funds for the Central Universities (Grant No. 22A201514019).

Reference

1. B. Tanhaei, A. Ayati, M. Lahtinen and M. Sillanpää, *Chem Eng J*, 2015, **259**, 1-10.
2. Y. Li, J. Sun, Q. Du, L. Zhang, X. Yang, S. Wu, Y. Xia, Z. Wang, L. Xia and A. Cao, *Carbohyd Polym*, 2014, **102**, 755-761.
3. M. Kousha, E. Daneshvar, M. S. Sohrabi, M. Jokar and A. Bhatnagar, *Chem Eng J*, 2012, **192**, 67-76.
4. L. Wang, X.-L. Wu, W.-H. Xu, X.-J. Huang, J.-H. Liu and A.-W. Xu, *Acs Appl Mater Inter*, 2012, **4**, 2686-2692.
5. A. Rodríguez, J. García, G. Ovejero and M. Mestanza, *Journal of Hazardous Materials*, 2009, **172**, 1311-1320.
6. N. Mahanta and J. P. Chen, *J Mater Chem A*, 2013, **1**, 8636-8644.
7. V. Njoku, K. Foo, M. Asif and B. Hameed, *Chem Eng J*, 2014, **250**, 198-204.
8. F. Liu, S. Chung, G. Oh and T. S. Seo, *Acs Appl Mater Inter*, 2012, **4**, 922-927.
9. X. Jin, B. Yu, Z. Chen, J. M. Arocena and R. W. Thring, *Journal of Colloid and Interface Science*, 2014, **435**, 15-20.
10. S. Luo, P. Qin, J. Shao, L. Peng, Q. Zeng and J.-D. Gu, *Chem Eng J*, 2013, **223**, 1-7.
11. P. Liu and L. Zhang, *Sep Purif Technol*, 2007, **58**, 32-39.
12. C. Gu, H. Jia, H. Li, B. J. Teppen and S. A. Boyd, *Environ Sci Technol*, 2010, **44**, 4258-4263.

13. D. Parasuraman and M. J. Serpe, *Acs Appl Mater Inter*, 2011, **3**, 2732-2737.

14. T. Feng and L. Xu, *RSC Adv.*, 2013, **3**, 21685-21690.

15. G. Dotto and L. Pinto, *Carbohyd Polym*, 2011, **84**, 231-238.

16. G. Dotto, J. Moura, T. Cadaval and L. Pinto, *Chem Eng J*, 2013, **214**, 8-16.

17. M. Auta and B. Hameed, *Chem Eng J*, 2014, **237**, 352-361.

18. F. Yu, L. Chen, J. Ma, Y. Sun, Q. Li, C. Li, M. Yang and J. Chen, *RSC Advances*, 2014, **4**, 5518-5523.

19 Z. Zhou, S. Lin, T. Yue and T.-C. Lee, *Journal of Food Engineering*, 2014, **126**, 133-141.

20. L. Zhou, J. Jin, Z. Liu, X. Liang and C. Shang, *Journal of Hazardous Materials*, 2011, **185**, 1045-1052.

21. G. Z. Kyzas, P. I. Siafaka, E. G. Pavlidou, K. J. Chrissafis and D. N. Bikiaris, *Chem Eng J*, 2015, **259**, 438-448.

22. X. Zhu, B. Li, J. Yang, Y. Li, W. Zhao, J. Shi and J. Gu, *Acs Appl Mater Inter*, 2014, **7**, 223-231.

23. X. Luo, C. Wang, L. Wang, F. Deng, S. Luo, X. Tu and C. Au, *Chem Eng J*, 2013, **220**, 98-106.

24. X. Li, Y. Qi, Y. Li, Y. Zhang, X. He and Y. Wang, *Bioresource Technology*, 2013, **142**, 611-619.

25. M. R. Gandhi, G. Kousalya, N. Viswanathan and S. Meenakshi, *Carbohyd Polym*, 2011, **83**, 1082-1087.

26. A. Varma, S. Deshpande and J. Kennedy, *Carbohyd Polym*, 2004, **55**, 77-93.

27 S. Mondal, C. Li and K. Wang, J. Chem. Eng. Data, 2015, 60, 2356-2362

28. Y. A. El-Reash, M. Otto, I. Kenawy and A. Ouf, *International journal of biological macromolecules*, 2011, **49**, 513-522.

29. G. Bayramoglu, B. Altintas and M. Y. Arica, *Chem Eng J*, 2009, **152**, 339-346.

30. Y. Wu, M. Zhang, H. Zhao, S. Yang and A. Arkin, *RSC Advances*, 2014, **4**, 61256-61267.

31. L. Abramian and H. El-Rassy, *Chem Eng J*, 2009, **150**, 403-410.

32. J. Zhou, C. Tang, B. Cheng, J. Yu and M. Jaroniec, *Acs Appl Mater Inter*, 2012, **4**, 2174-2179.

33. S. Bouzid, A. Khenifi, K. Bennabou, R. Trujillano, M. Vicente and Z. Derriche, *Chemical Engineering Communications*, 2015, **202**, 520-533.

529

530 ## Figure captions

531 **Scheme 1:** The stuctures of chitosan and glutaraldehyde.

532 **Fig. 1:** FT-IR (A) spectra and XRD patterns (B) of CTS, CTS@Zr and CTS@-Zr-OII,
533 SEM images and EDS spectra of CTS@Zr microcomposite before (C, E) and after (D,
534 F) adsorption of Orange II dyes, respectivley.

535 **Fig. 2:** (A) Effect of pH (left) on Orange II dyes adsorption (100 and 50 mg L^{-1} of
536 Orange II (100 mL), 20 mg of dosage and 303 K.) and zeta potential study (right) for
537 CTS@Zr microcomposite (50 mg dosage, pH=1~11, 100 mL 0.01 mol L^{-1} KNO_3 and
538 298 K); (B) Adsorption capacity of Orange II on different amount of Zr^{4+} (left) and
539 the leaching concentration of Zr into solution at pH 1 (right). (100 mg L^{-1} of Orange II
540 (100 mL), 20 mg of dosage and 303 K.)

541 **Fig. 3:** (A) Effect of contact time on adsorption capacity of Orange II dyes; (B)
542 pseudo-second-order kinetics under different temperature conditions (277, 293, 303
543 and 313 K) and (C) the plot of ln K_L *vs.* 1/T. (pH=2, 200 mg L^{-1} of Orange II (100
544 mL), 20 mg of dosage.)

545 **Fig. 4:** Adsorption isotherms of the Orange II dye adsorption onto CTS@Zr
546 microcomposite (A), the cure of Ce/Co vs Co (B) and images of removal effect with
547 different initial dyes concentrations (50 ~ 300 mg L^{-1}). (pH=2, 100 mL of Orange II,
548 20 mg of dosage and 303 K.)

549 **Fig. 5:** The adsorption cpacities for Orange II dyes at range of pH 1-12 for CTS,
550 CTS-GL and CTS@Zr microcomposite. (100 mg L^{-1} of Orange II (100 mL), 20 mg of

dosage and 303 K.)

Fig. 6: Desorption process of Orange II from the CTS@Zr microcomposite OII using 0.05 M NaOH and reusability of CTS@Zr microcomposite for Orange II dyes (inset figure)

Scheme 2: The possible of adsorption mechanism of Orange II dyes using CTS@Zr microcomposit.

Tables

Table 1

The results of BET analysis and EDS analysis for CTS@Zr microcomposite

	BET surface area (m^2 g^{-1})	Micropore surface area (m^2 g^{-1})	External surface area (m^2 g^{-1})	Average pore size (nm)
BET Analysis	6.24	48.0	8.69	32.4

	Element	C	N	O	Zr	Cl	S
EDS Analysis	CTS@Zr	32.6	4.78	32.6	27.5	2.61	—
	CTS@Zr-OII	38.4	5.40	32.2	18.5	—	5.53

Table 2

Kinetics and thermodynamics parameters for the adsorption of OII on CTS@Zr microcomposite at different temperatures

T	pseudo-first-order model			pseudo-second-order model			Thermodynamics parameters			
(^{o}C)	q_{m1} (mg g^{-1})	$k_1\times10^3$ ($min^{-1)}$	R^2	q_{m2} (mg g^{-1})	$k_2\times10^6$ (g (mg·min)$^{-1}$)	R^2	q_{exp} (mg g^{-1})	ΔH (kJ mol^{-1})	ΔS (kJ (mol·K)$^{-1}$)	ΔG (kJ mol^{-1})
4	420	1.31	0.988	534	5.11	0.994	525			-4.471
20	612	1.26	0.930	908	6.68	0.990	898			-8.939
30	520	1.01	0.945	932	4.86	0.996	926	57.3	0.223	-10.27
40	394	1.60	0.850	955	10.4	0.999	951			-12.50

Table 3

The parameters of Langmuir, Freundlich and Temkin isotherm models for the adsorption of Orange II dyes on CTS@Zr microcomposite

Temkin			Freundlich		
B (J mol^{-1})	A_T (L g^{-1})	R^2	k_F (L g^{-1})	n	R^2
95.7	273	0.939	517	6.75	0.903
Langmuir					
q_m (mg g^{-1})		k_L(L mg^{-1})	R^2	R_L	
926		0.16	0.999	0.02-0.11	

Table 4

Comparison the maximum adsorption capacity of OII onto various adsorbents

Adsorbents (S_{BET}, m^2 g^{-1})	Adsorption capacity (mg g^{-1})	Reference
Zirconium-based chitosan microcomposite (6.24)	926 (30 ^oC)	This work
activated carbon (997)	569 (65 ^oC)	5
Hexadecyltrimethylammonium bromide (HDTMA)-coated zeolite (400)	39 (30 ^oC)	9
Poly (N-isopropylacrylamide) microgels (--)	49 (room temperature)	13
NH_2-MCM-41(921)	278 (25 ^oC)	30
Porous titania aerogel (500)	420 (30 ^oC)	31
Rattle-type carbon−alumina core−shell spheres (182)	209 (25 ^oC)	32
Phosphonium-modified Algerian bentonites (--)	53.8 (20 ^oC)	33

633

634 Table 5:

635 Compared the adsorption performances of equilibrium time, adsorption capacity and

636 remove rate among of CTS, CTS-GL and CTS@Zr microcomposite.

Adsorbents	Equilibrium time (h)	Adsorption capacity (mg g^{-1})	Remove rate (%)
CTS	28	186	37.2
CTS-GL	14	122	24.4
CTS@Zr	10	497	99.4

637

638

639

640

641

642

643

644

645

646

647

648

649

650

651

Graphical Abstract, Schemes and Figures

Graphical Abstract

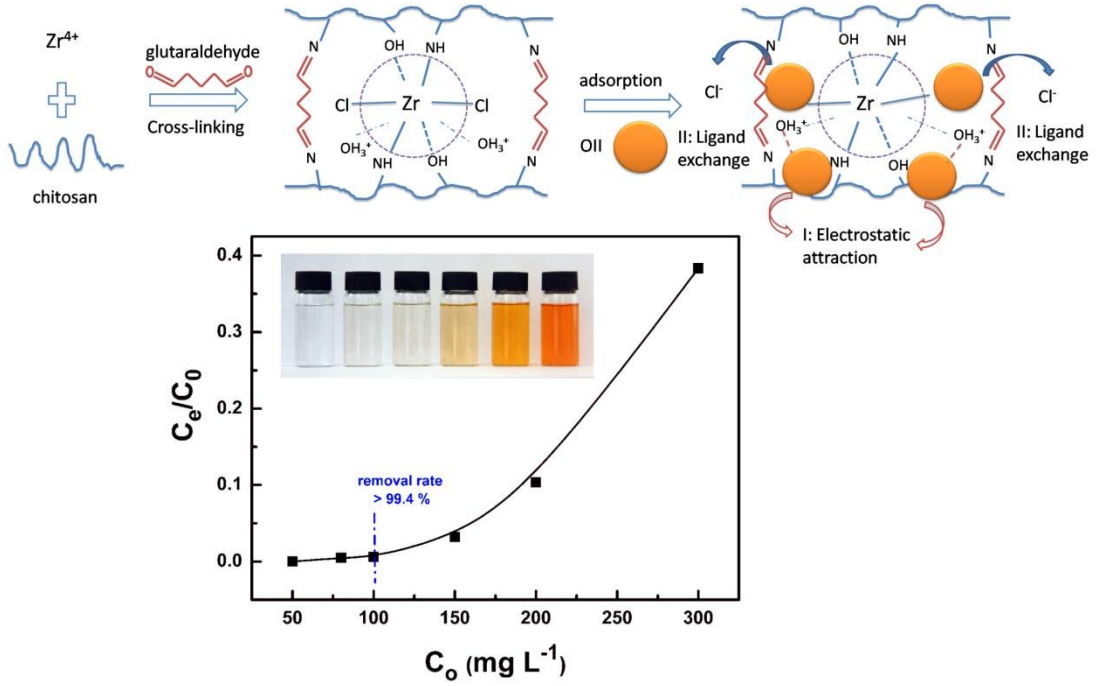

Scheme 1

Chitosan

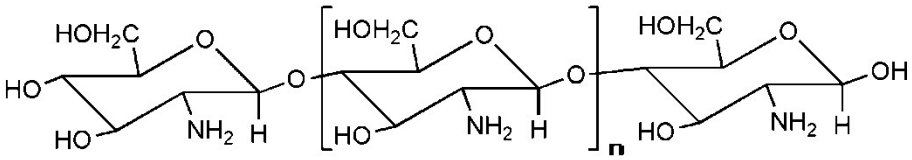

Glutaraldehyde

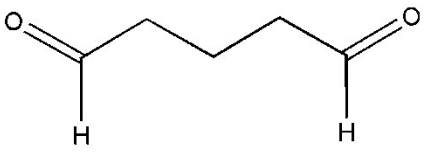

662

663 Fig. 1

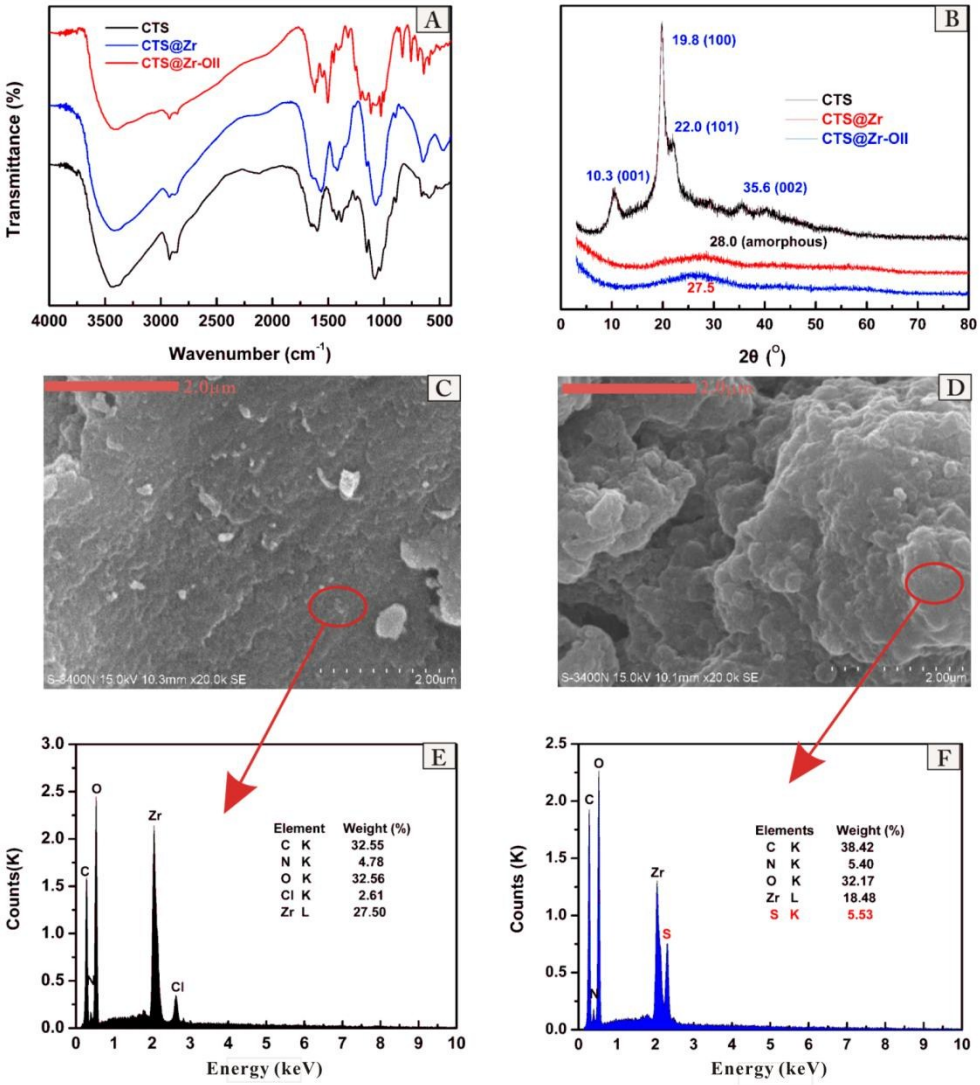

664

665

666

667

668

669

670

Fig. 2

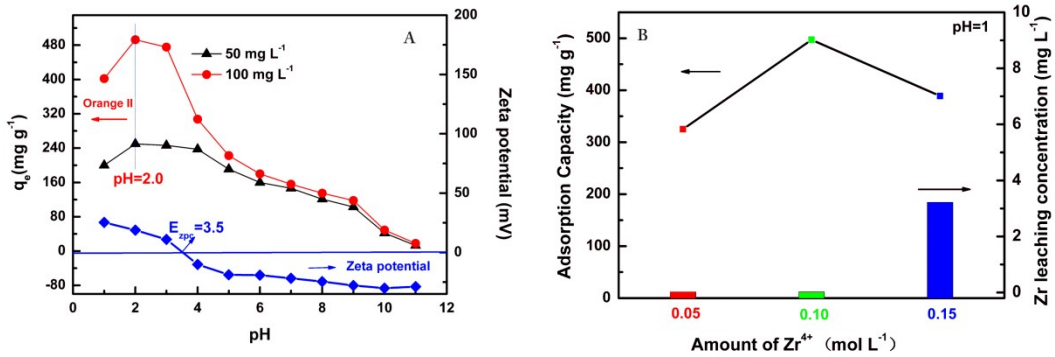

Fig. 3

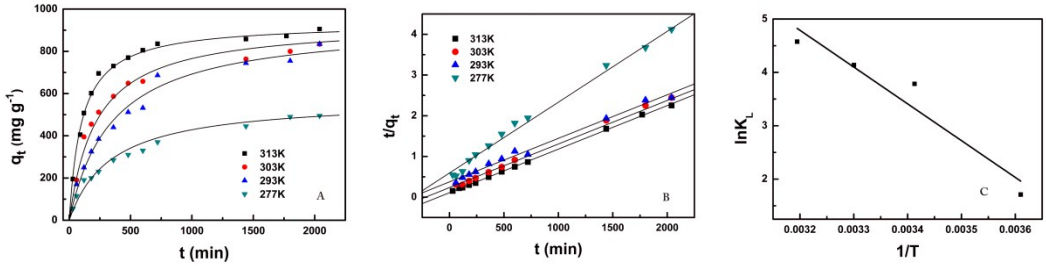

686

687 Fig. 4

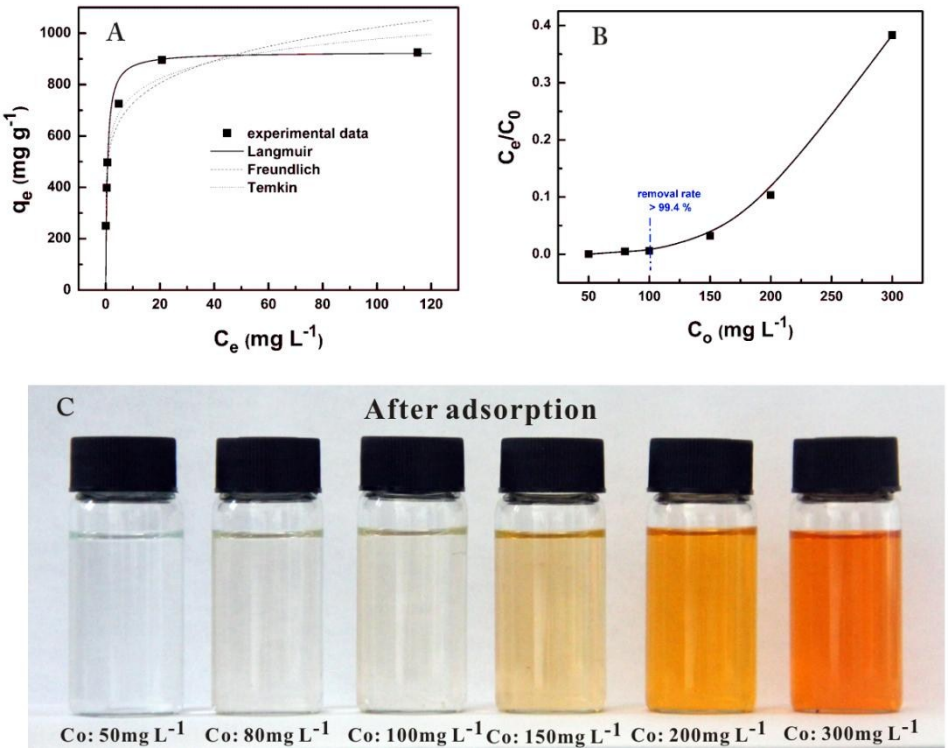

688

689

690 Fig. 5

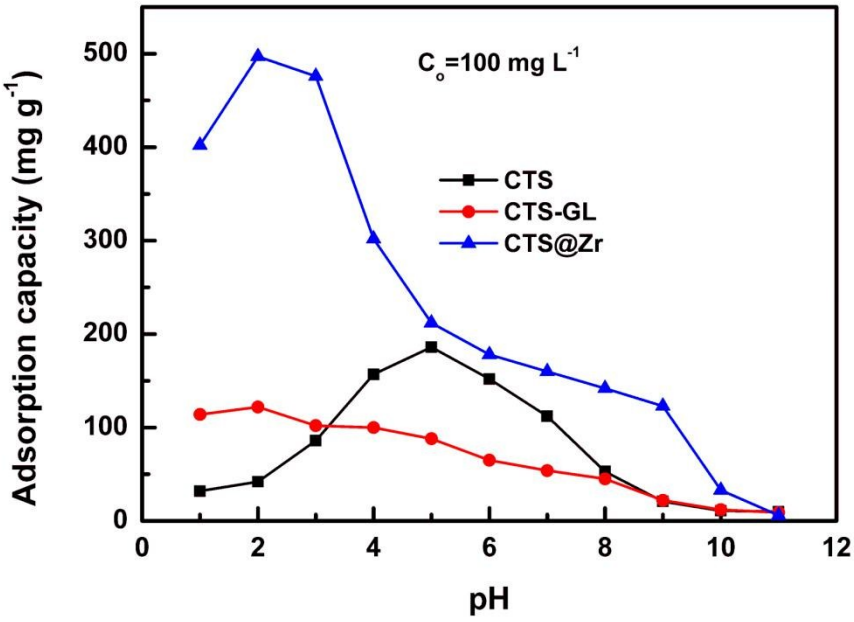

691

692

693 Fig. 6

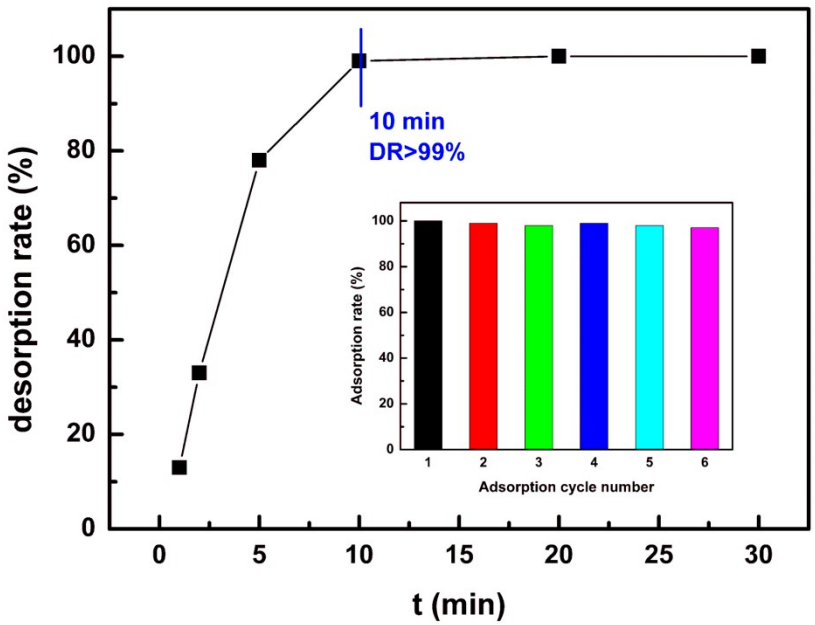

694

695

696 Scheme 2

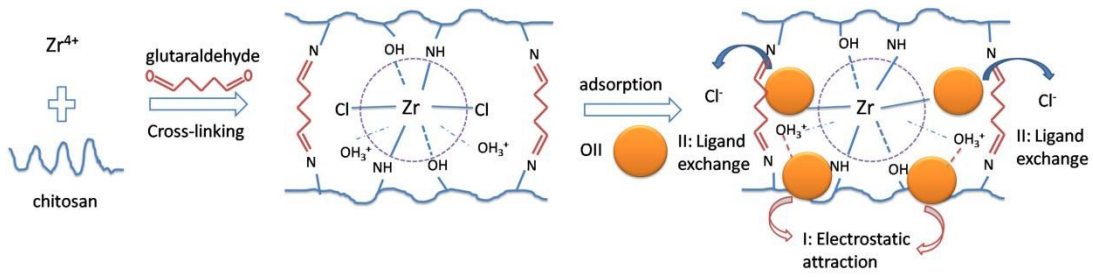

697